Conformational Switching between Protein Substates Studied with 2D IR Vibrational Echo Spectroscopy and Molecular Dynamics Simulations

Sayan Bagchi,[†,⊥] Dayton G. Thorpe,[‡,§,⊥] Ian F. Thorpe,[‡,∥] Gregory A. Voth,[*,‡] and M. D. Fayer[*,†]

Department of Chemistry, Stanford University, Stanford, California 94305, United States, and Department of Chemistry, James Franck Institute, and Computation Institute, University of Chicago, 5735 South Ellis Avenue, Chicago, Illinois 60637, United States

Received: September 26, 2010; Revised Manuscript Received: October 27, 2010

Myoglobin is an important protein for the study of structure and dynamics. Three conformational substates have been identified for the carbonmonoxy form of myoglobin (MbCO). These are manifested as distinct peaks in the IR absorption spectrum of the CO stretching mode. Ultrafast 2D IR vibrational echo chemical exchange experiments are used to observed switching between two of these substates, A_1 and A_3, on a time scale of <100 ps for two mutants of wild-type Mb. The two mutants are a single mutation of Mb, L29I, and a double mutation, T67R/S92D. Molecular dynamics (MD) simulations are used to model the structural differences between the substates of the two MbCO mutants. The MD simulations are also employed to examine the substate switching in the two mutants as a test of the ability of MD simulations to predict protein dynamics correctly for a system in which there is a well-defined transition over a significant potential barrier between two substates. For one mutant, L29I, the simulations show that translation of the His64 backbone may differentiate the two substates. The simulations accurately reproduce the experimentally observed interconversion time for the L29I mutant. However, MD simulations exploring the same His64 backbone coordinate fail to display substate interconversion for the other mutant, T67R/S92D, thus pointing to the likely complexity of the underlying protein interactions. We anticipate that understanding conformational dynamics in MbCO via ultrafast 2D IR vibrational echo chemical exchange experiments can help to elucidate fast conformational switching processes in other proteins.

I. Introduction

Structural changes in proteins are essential for many biological functions. Different conformations influence protein−ligand interactions[1] and play a role in enzyme catalysis.[2,3] Protein folding or unfolding involves a large number of major structural changes. Global protein conformational transformations occurring on time scales of microseconds and longer may be collectively composed of much faster, individual motions that can take place on the time scale of tens of picoseconds.[1,4] Molecular dynamics (MD) simulations are frequently employed to study structural changes involved in problems such as protein folding. To assess the ability of MD to straightforwardly describe the time dependence of protein structural evolution, it is useful to study a single well-defined structural change that is accessible to both experiment and simulation. Indeed, such MD simulations may be limited by several factors, such as the accuracy of the underlying potential energy function, relatively short simulation time scales and related equilibration issues, and a lack of knowledge of the proper collective coordinate(s) to sample for the protein conformational changes. All of these challenges make a comparison with detailed experimental result invaluable to improve ultimately the accuracy and applicability of the MD simulation technology.

The protein myoglobin, a small globular heme protein, is a useful system for studying fast protein conformational changes.[4,5] Three conformational substates[3] have been identified for the carbonmonoxy form of myoglobin (MbCO) that are reflected by the IR absorption bands of the CO stretching mode. The three substates give rise to three peaks in the absorption spectrum referred to as A_0 (1965 cm^{-1}), A_1 (1945 cm^{-1}), and A_3 (1932 cm^{-1}).[5−7] The proximate cause of the different MbCO substates is thought to arise from the configuration of the imidazole side group of the distal histidine, H64.[1,8] Structural changes in the protein cause the side group to occupy three distinct positions. Conformational switching between the A_0 substate and either the A_1 or A_3 substate has been indirectly estimated to take place on the $1-10$ μs time scale.[4] In the A_0 substate, the imidazole has swung out of the heme pocket.[4] Both the A_1 and A_3 substates have the imidazole in the pocket. In all three substates, the ε-nitrogen of the imidazole is protonated, and the δ-nitrogen is deprotonated.[1] In the A_3 substate, the protonated nitrogen is close to the CO, whereas in the A_1 substate, it is further from the CO.[1,8] The differences in the locations of the imidazole side group of H64 give rises to the CO stretch spectral shifts associated with the three substates.

Direct observation of the switching between the A_1 and A_3 substates in the myoglobin mutant L29I has been accomplished using ultrafast 2D IR vibrational echo chemical exchange spectroscopy.[4,9] The 2D IR vibrational echo technique is akin to 2D NMR, but it operates on much faster time scales. As

* Correponding authors. E-mail: fayer@stanford.edu (M.D.F.); gavoth@uchicago.edu (G.A.V.).
† Stanford University.
‡ University of Chicago.
§ Present address: Department of Physics & Astronomy, University of Southern California.
∥ Present address: Department of Chemistry & Biochemistry, University of Maryland, Baltimore County.
⊥ These authors contributed equally to this work.

10.1021/jp109203b
Published on Web 12/03/2010

discussed below, the substate switching time (chemical exchange) is determined by the growth of off-diagonal peaks in the 2D IR spectrum. The time constant for interconversion between the L29I A_1 and A_3 substates is 47 ± 8 ps.[4] Substate switching in wild-type MbCO has not been observed because the A_1 band has much larger amplitude than the A_3 band. The A_3 band appears as a small shoulder on the A_1 absorption. In L29I, the A_1 and A_3 bands overlap, but they are approximately the same size, making the observation of off-diagonal peaks in the 2D IR spectrum possible.

In this Article, we report the observation of A_1-A_3 substate switching in another Mb mutant, a double mutant T67R/S92D. In this mutant, the A_3 band is somewhat larger than the A_1 band in the absorption spectrum, but both have sufficient amplitude to make observation of the growth of off-diagonal peaks in the 2D IR spectrum possible. As shown below, the time constant for interconversion between the T67R/S92D A_1 and A_3 substates is 76 ± 10 ps.

Interconversion from one substate to another requires crossing a barrier that is non-negligible at room temperature. The measurements of the substate interconversion times for the two mutants, L29I and T67R/S92D, can serve as an important test of predictions derived from MD simulations. The time scale of the substate interconversions, along with the small size of MbCO and the availability of atomic-resolution crystal structures,[10,11] make substate interconversion in MbCO readily addressable by MD simulations. The existence of conformational substates in MbCO was first identified in MD simulations in 1987.[12] Devereux and Meuwly[13] have used electronic structure methods combined with MD simulations using the CHARMM force field to investigate spectroscopic substates of wild-type Mb. Their calculations do not support the interpretation of the structures associated with the A_1 and A_3 substates in wild-type Mb[1,8] but also do not produce any candidate structures consistent with the experimentally observed dominant A_1 substate. Recent MD simulations of the double mutant discussed here[14] using the Amber 10 simulation package with the 2003 force field,[15,16] are consistent with the previous interpretation of the A_1 and A_3 substates in wild-type Mb.[1,8]

The experimental measurement of the interconversion time between the A_1 and A_3 substates offers a new way to check a given computational model. Reproducing the A_1-A_3 interconversion time in MD simulations would be an important milestone, demonstrating that "the dynamics of real systems undergoing an elementary structural change can be reproduced" and providing structural details of the A_1-A_3 interconversion.[4] In addition to the experiments on the double mutant T67R/S92D, the study presented below uses MD simulations in concert with umbrella sampling and the weighted histogram analysis method[17] to investigate the free energy landscape and structural differences between the A_1 and A_3 substates of L29I and T67R/S92D MbCO. The experimental time constants of both Mb mutants were compared with those obtained from the simulations. It was found that the simulations were able to reproduce the L29I substate interconversion time constant with good accuracy, but the same approach when applied to the T67R/S92D double mutant produced results that are not consistent with the time-dependent 2D IR spectroscopy nor with the IR linear absorption spectrum.

II. Computational and Experimental Procedures

A. Computational Methods. MD simulations were performed using the CHARMM software package[18] with the CHARMM22 force field.[19] A nonstandard parameter set was used for the heme group partial charges in accordance with the parameter set suggested by Devereux and Meuwly.[13] This parameter set has a net charge of -2, so extra positive charge was added evenly to all atoms in the heme group to generate a net charge of 0. Grossfield's WHAM code was used to calculate potentials of mean force (PMFs) from the umbrella sampling data.[20] All simulations began from the wild-type crystal structure 1a6g,[10] with the L29I or T67R/S92D mutations then implemented manually and hydrogen atoms added by CHARMM. The distal histidine is simulated with N_ε protonated and N_δ deprotonated. Before solvation, both systems underwent 5000 steps of steepest descent minimization, followed by solvation and the addition of two chloride ions for electroneutrality, followed by an additional 5000 steps of steepest descent energy minimization. Both systems were solvated in a truncated octahedron of additional solvent with side length equal to ~67 Å, which kept the protein a minimum of 9 Å away from the edge of the water box to prevent it from interacting with its periodic image, in addition to the water molecules found in the crystal structure 1a6g. For the L29I system, 7488 water molecules were added. For the T67R/S92D system, 7431 water molecules were added. Hydrogen bond lengths were fixed using the SHAKE algorithm.[21]

For the L29I mutant, before any biasing potentials were added, the energy-minimized system was equilibrated for slightly over 6.4 ns. For the C_α-C_β-C_γ-$C_{\delta 2}$ dihedral angle, 18 windows were used, biased in 20° increments. Each window ran for 2 ns, including equilibration time after the bias was applied. For the N_ε-O distance, 23 windows were used, biased in 0.1 Å increments from 2.7 to 4.9 Å. Again, each window ran for 2 ns, including equilibration after the bias was applied. For the N_δ-O distance, 25 windows were used, biased in 0.1 to 0.25 Å increments from 3.0 to 6.375 Å. The N_δ-O biased windows ran between 1.4 and 3.8 ns.

For the T67R/S29D mutant, before any biasing potentials were added, the energy-minimized system was equilibrated for 4.0 ns. For the C_α-C_β-C_γ-$C_{\delta 2}$ dihedral angle, 18 windows were used, biased in 20° increments. Each window ran for 4 ns, including equilibration time after the bias was applied. For the N_ε-O distance, 14 windows were used, biased in 0.25 Å increments from 2.75 to 6.0 Å. Each window ran for between 2.13 and 3.73 ns, including equilibration time after the bias was applied. For the N_δ-O distance, 16 windows were used, biased in increments of 0.25 or 0.125 Å from 3.0 to 6.0 Å. Three of those windows ran for 1.47 ns, and the other 13 windows ran for 4 ns. All biased windows used a harmonic biasing potential with an amplitude of 10 kcal/mol. The constant NVT ensemble was employed, with all simulations executed at a temperature of 300 K. Every 2 ps, the velocities of all atoms were randomly reassigned to fit the system temperature to within 5 K of 300 K. Periodic boundary conditions were used. Electrostatics were calculated using the particle mesh Ewald algorithm,[22] whereas nonbonded interactions were truncated at 10 Å with a 1 Å buffer for the FSHIFT and VSWITCH functions. Integration of the dynamics was carried out using the velocity Verlet integrator and 2 fs time steps. Trajectories were saved every 2 ps for later analysis.

B. Experimental Methods. 2D IR vibrational echo chemical exchange spectroscopy,[4,9] which is an IR analog of 2D NMR, was used for the determination of the conformational switching rate of L29I[4] and T67R/S92D. Experimental details of 2D IR vibrational echoes and chemical exchange spectroscopy have been previously described.[9,23−25] In a 2D IR vibrational echo experiment, three ultrashort IR pulses tuned to the vibrational

absorption frequency of A_1 and A_3 are crossed in the sample. The IR excitation pulses (110 fs in duration and 150 cm^{-1} fwhm) are produced using a Ti/sapphire regenerative amplifier pumped optical parametric amplifier system.[26] These pulses have sufficient bandwidth to excite the CO stretching vibrational modes of both A_1 and A_3 simultaneously. The first pulse "labels" the initial structures of the species by labeling their initial frequencies, ω_τ. The second laser pulse ends the first time period and starts the evolution period T_w during which the labeled species undergo conformational switching and vibrational relaxation to the ground state. The third pulse ends the evolution period and induces the vibrational echo emission, which reports on the structures that exist at the end of T_w by their final frequencies (ω_m).

In the 2D IR spectra, ω_τ is the horizontal axis and ω_m is the vertical axis. At short time, two positive going peaks are on the diagonal at the A_1 and A_3 0−1 CO vibrational absorption frequencies. There are two more peaks that are directly below the A_1 and A_3 peaks. These are negative going peaks and correspond to vibrational echo emission at the frequency of the 1−2 vibrational transitions of the A_1 and A_3 CO stretch. These peaks are shifted to lower frequency along the ω_m frequency by the vibrational anharmonicity.[27,28] In the absence of chemical exchange, the peaks in the spectrum will evolve in shape because of spectral diffusion that was caused by structural fluctuations within the individual MbCO[29,30]substates. The peaks will also decay because of the vibrational lifetimes of the CO stretching mode of each substate.

Chemical exchange, where two species in equilibrium interconvert one to another without changing the overall number of the species, also contributes to the 2D IR vibrational echo spectrum.[9] Chemical exchange causes additional off-diagonal peaks to grow in during the T_w period.[9] The interconversions between the A_1 and A_3 substates for L29I[4] and T67R/S92D are examples of chemical exchange. In the 0−1 region of the 2D spectrum, when proteins initially in the A_1 substate convert to the A_3 substate, a new peak appears with the A_1 frequency on the ω_τ axis but with the A_3 frequency on the ω_m axis. In the same manner, when proteins initially in the A_3 substate convert to the A_1 substate, a new peak appears with the A_3 frequency on the ω_τ axis but with the A_1 frequency on the ω_m axis. Analysis of the growth of these off-diagonal peaks with increasing T_w gives the chemical exchange rate.[9] Because the system is in equilibrium, the two off-diagonal peaks, $A_1 \rightarrow A_3$ and $A_3 \rightarrow A_1$, grow in at the same rate. In the 1−2 region of the spectrum, equivalent off-diagonal peaks grow in.[9]

If the vibrational anharmonicity is large compared with the frequency difference of the two species undergoing chemical exchange, then two blocks of nonoverlapping peaks appear in the 2D IR vibrational echo chemical exchange spectrum.[9] One block in the 0−1 region of the spectrum has the two positive peaks on the diagonal and two positive peaks off-diagonal. The block in the 1−2 region looks the same, but it is shifted by the anharmonicities and is negative going.[9] In the data presented below for the MbCO double mutant T67R/S92D and in the data previously reported for the L29I single mutant,[4] the anharmonicity is not large. Therefore, some of the negative going peaks overlap with positive going peaks. This complicates the appearance of the spectrum but does not inhibit the analysis of the chemical exchange rate.

III. Results and Discussion

A. Double-Mutant Substate Switching Measurements. The background-subtracted linear absorption spectrum of CO bound to the Myoglobin double mutant T67R/S92D is shown in Figure 1 (solid curve) along with the result of fitting the spectrum to two Gaussians (dashed curves). The two Gaussians reflect the two spectroscopically distinct conformational substates, A_1 at 1945 $cm^{-1}$and A_3 at 1933 cm^{-1}. The positions of the peaks are the same as those observed in wild-type MbCO within experimental error. However, in wild-type MbCO, the A_1 substate dominates the spectrum, and the A_3 substate is a small shoulder on the low-frequency side of the band. In the MbCO double mutant, the A_3 band has more amplitude. In the L29I single mutant, the two bands are approximately the same amplitude.[4] The mutations do not significantly shift the absorption frequencies of the CO stretching mode in the two substates, but the mutations do change the relative amplitudes of the bands.

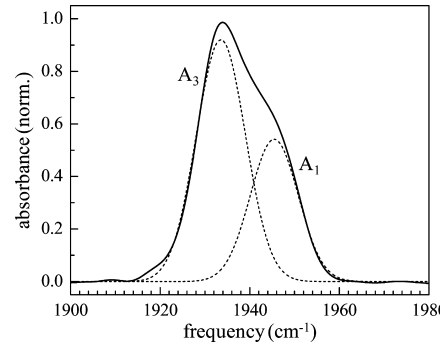

Figure 1. FT-IR spectrum of the CO stretch of heme-ligated CO for the myoglobin double mutant T67R/S92D (solid curve). The spectrum was fit with two Gaussians (dashed curves), which represent the absorption bands of the A_1 and A_3 substates. The peak positions are the same as those found in wild-type MbCO.

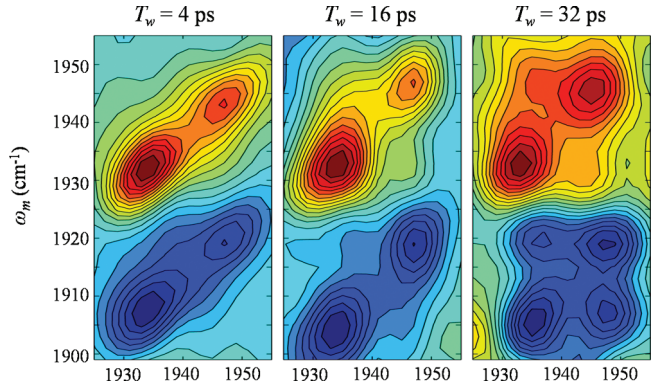

Figure 2. 2D IR spectra of CO bound to the Mb double-mutant T67R/S92D at several waiting times (T_w). The bands in the upper half of the spectrum (red) correspond to the 0−1 vibrational transition. The bands in the lower half of the spectrum (blue) arise from the vibrational echo emission at the 1−2 transition frequency.

Examples of the 2D IR vibration echo spectra are shown in Figure 2 at three of the waiting times (T_w) that were measured in the experiments. Each spectrum is normalized to the largest peak. The bands in the upper half of the spectrum correspond to the 0−1 transitions (red, positive going), and those in the lower half correspond to vibrational echo emission at the 1−2 transitions (blue, negative going). As discussed above, the 1−2 peaks are displaced along the ω_m vertical axis to lower frequency by the anharmonic shift of the CO stretch. The prominent red peaks correspond to the two peaks in the linear absorption spectrum in Figure 1. The peak centered at (ω_τ, ω_m) = (1932, 1932 cm^{-1}) arises from the A_3 substate, and that at (ω_τ, ω_m) = (1945, 1945 cm^{-1}) is from the A_1 substate. Off-diagonal peaks between the A_1 and A_3 substates in the 0−1 and 1−2 region grow in with increasing waiting time T_w, which is the signature

of A_1-A_3 conformational switching. In the $T_w = 32$ ps spectrum, the off-diagonal peaks have become substantial. Because the anharmonicity is not sufficiently large, there is overlap of the positive going 0−1 and negative going 1−2 bands that distorts the amplitudes of the other two off-diagonal peaks at $(\omega_\tau, \omega_m) = (1945, 1932\ cm^{-1})$ and $(\omega_\tau, \omega_m) = (1932, 1920\ cm^{-1})$. The overlap of the bands does not interfere with the analysis because the locations of all peaks are known, and all of the off-diagonal chemical exchange peaks grow in at the same rate.[9] In the analysis, it is also necessary to know the vibrational lifetimes of the CO stretch in the two substates. Lifetimes of the substates were measured using IR pump−probe experiments. The lifetimes for A_1 and A_3 are 22 and 20 ps, respectively.

Structural fluctuations of the protein produce spectral diffusion within each substate. Spectral diffusion changes the shapes of the bands but does not change their volume.[9] Substate switching causes the 0−1 diagonal peaks and the corresponding 1−2 peaks to decrease in volume, whereas the off-diagonal chemical exchange peaks increase in volume. The vibrational lifetime of the CO stretch, T_1, causes all peaks to decrease in volume. Unlike small molecules in liquids,[9,25,31−36] the orientational relaxation in the protein is slow and can be neglected.[4] The integrated peak volumes were determined by fitting all of the peaks to 2D Gaussian functions.[9,23] The resulting fits were used to extract the time constant for the conformational switching from the 2D spectra.[9,23]

Equation 1 shows the kinetic model used to determine the rate of the A_1-A_3 interconversion.

$$\xleftarrow{1/T_{1A_1}} A_1 \underset{k_{31}}{\overset{k_{13}}{\rightleftharpoons}} A_3 \xrightarrow{1/T_{1A_3}} \qquad (1)$$

$T_{1A_1}$and T_{1A_3} are the vibrational lifetimes of the two substates. As the system is in thermal equilibrium, the k_{13} and k_{31} exchange rate constants in eq 1 are equal. The ratio of the substate concentrations $[A_1]/[A_3]$ at equilibrium (the equilibrium constant) was determined from 2D IR peak volumes at very short time and from the FTIR spectrum, $[A_1]/[A_3] = 0.75$. Because $k_{13} = k_{31}$ and the equilibrium constant and the lifetimes are known, the data can be fit with a single adjustable parameter, the $A_1 \rightarrow A_3$ substate switching time, $\tau_{13} = 1/k_{13}$. The detailed fitting procedure involving all eight peak volumes obtained from the 2D IR chemical exchange spectrum has been previously described[9,23]

Figure 3 shows the plot of the experimental diagonal and off-diagonal peak volumes for 0−1 transition. The solid lines are obtained by fitting the data to the kinetic model with τ_{13} as the single adjustable parameter. Note that the off-diagonal exchange peak data and fit have been multiplied by three for clarity. The data from the 1−2 bands can be reproduced using the parameters obtained from the 0−1 region fits, demonstrating that the thermal equilibrium of the system is not perturbed by the vibrational excitation of the CO stretch within experimental error.[9] The fitting results yield $\tau_{13} = 76 \pm 10$ ps for the double mutant T67R/S92D. The value for the single mutant L29I is 47 ± 8 ps.

B. MD Simulations. On the basis of previous studies, it is believed that the configuration of the distal histidine, His64, is the most important structural factor influencing the vibrational frequency of the A_1 and A_3 substates.[1,4,14] The simulations in the present work were used to determine the PMFs along three structural coordinates describing the configuration of His64 relative to the CO ligand: the separation distance between the

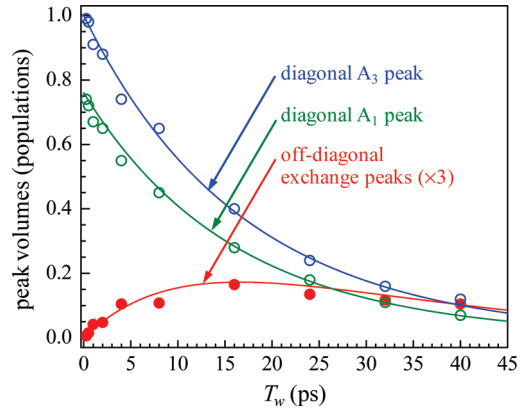

Figure 3. Peak volume data obtained from the fitting of the 2D IR spectra of T67R/S92D for the 0−1 transition region. The solid curves are the results of the fit to the kinetic model with one adjustable parameter. The results yield the A_1 to A_3 substate switching time $\tau_{13} = 76 \pm 10$ ps.

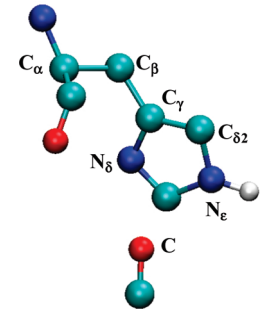

Figure 4. His64 and the nearby CO ligand. Hydrogen atoms are suppressed except for N_ε-H; N_δ is not protonated.

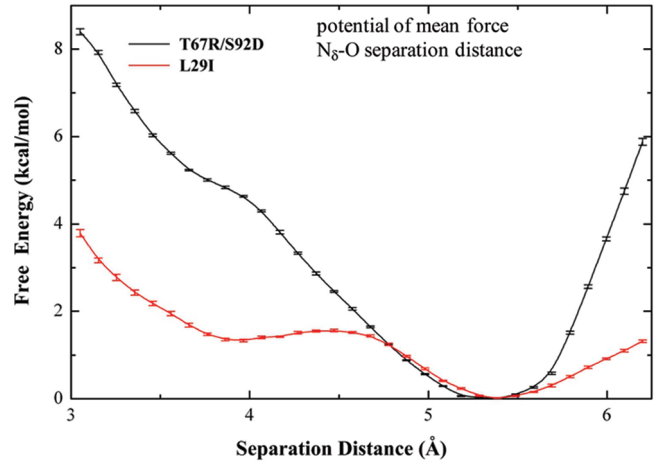

Figure 5. Potential of mean force for the N_δ-O separation distance. The black line corresponds to L29I MbCO. The red line corresponds to T67R/S92D MbCO.

δ-nitrogen (N_δ) of His64 and the oxygen atom of the CO ligand (N_δ-O), the separation distance between the ε-nitrogen (N_ε) of His64 and the oxygen atom of the CO ligand (N_ε-O), and the C_α-C_β-C_γ-$C_{\delta 2}$ dihedral angle of the distal histidine's imidazole side chain relative to its backbone (see Figure 4).

Results for the L29I mutant will be considered first. These simulations display substate interconversion most clearly in the PMF for the N_δ-O distance. (See Figure 5.) Along this coordinate, the energy barrier for the rate-limiting step, escaping the minimum that is deepest at 5.4 Å, is 1.56 kcal/mol. The energy barrier to back reaction is 0.23 kcal/mol. From transition-state theory, we can estimate the substate interconversion frequency as

$$K = \frac{\omega_0}{2\pi} \exp\left(\frac{\Delta F}{K_b T}\right) \quad (2)$$

where K is the reaction constant, K_b is the Boltzmann constant, T is the temperature of the simulations, ω_0 is the fundamental frequency, and ΔF is the free-energy barrier.[37] The fundamental frequency is calculated as $\omega_0 = [(d^2\mathrm{PMF}(r)/dr^2)/(m_{\mathrm{eff}})]^{1/2}$ where $m_{\mathrm{eff}} = (K_b T)/(\langle v^2 \rangle)$ and v is the time rate of change of the N_δ-O separation distance. The effective reaction coordinate velocity v was determined from unbiased MD trajectories in which the protein stayed near the free-energy minimum. This treatment assumes that the fundamental frequency can be described by an "effective force constant" related to the fluctuations of the reaction coordinate. The value of the second derivative of the PMF at the lower-energy minimum based on the best-fit sixth-order polynomial is 8.48 kcal mol^{-1} Å^{-2}, and the average velocity squared is 4.65 × 10^{22} Å^2 s^{-2}.

From these values, the reaction frequency in the deeper minimum is 9.42 × 10^9 s^{-1}, which corresponds to an interconversion time of 106 ps, a factor of 2.2 longer than the experimentally observed time of 47 ps for the L29I mutant. Around the higher energy minimum, the second derivative of the PMF is 3.04 kcal mol^{-1} Å^{-2}, and the average velocity squared is 4.95 × 10^{22} A^2 s^{-2}. The reaction frequency in the higher energy minimum near 3.96 Å is 5.43 × 10^{10} sec^{-1} for an interconversion time of 18.4 ps, shorter than the experimentally observed time for the L29I mutant by a factor of 2.6. Because of the exponential dependence of the reaction constant on the height of the energy barrier, the agreement within approximately a factor of 2 between the predicted and experimentally observed interconversion times may indicate that there is closer agreement between the predicted and actual energy barrier to substate interconversion along the N_δ-O separation distance than there is between the predicted and observed interconversion times. The only previous estimate in this range was 100−200 ps, based on 39 unbiased trajectories totaling 12.7 ns, which was not sufficient to provide a more precise estimate or a potential energy landscape along the path between the substates.[1] The ratio of the interconversion rate constants is the equilibrium constant. The equilibrium constant determines the ratio of the peak areas in the IR absorption spectrum. The ratio from the simulations is 5.8, whereas the experimental ratio is 1.1[4]

Computational studies of wild-type MbCO have suggested that rotation of the imidazole side chain of His64 may characterize the change between the A_1 and A_3 substates.[1] The simulations carried out in the present study do not show evidence of rotation of the imidazole ring in this interconversion. Rotation of the imidazole ring would most clearly be seen in the PMF of the C_α-C_β-C_γ-$C_{\delta 2}$ dihedral angle (Figure 6). Although the PMF for this coordinate for each mutant does clearly show two favorable positions, the higher energy minimum around 10° is so energetically unfavorable that the probability of finding the protein in a configuration with this dihedral angle between −30 and 162° is <1% for both the L29I mutant and the T67R/S92D mutant, making the higher energy minimum statistically insignificant.

The prediction that the A_1 and A_3 substates are differentiated by rotation of the imidazole side chain also requires that the N_ε-O separation distance have two favorable values.[1] However, the PMF for the N_ε-O separation distance displays only one favorable position for both of the mutants (Figure 7). For the L29I mutant, these results indicate that the His64 backbone moves laterally around the CO ligand in such a way that the

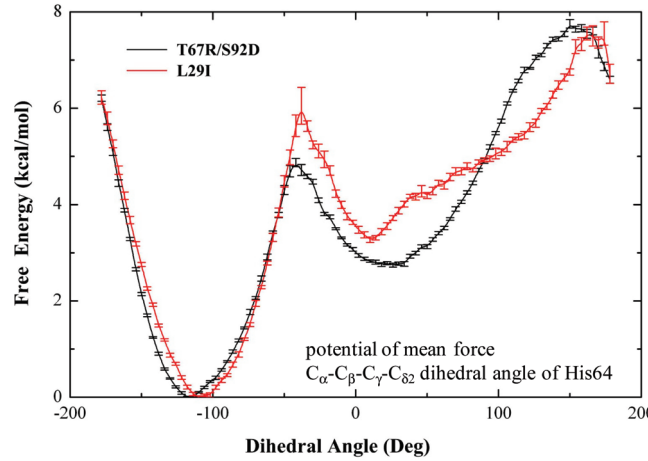

Figure 6. Potential of mean force for the C_α-C_β-C_γ-$C_{\delta 2}$ dihedral angle of His64. The black line corresponds to L29I MbCO. The red line corresponds to T67R/S92D MbCO.

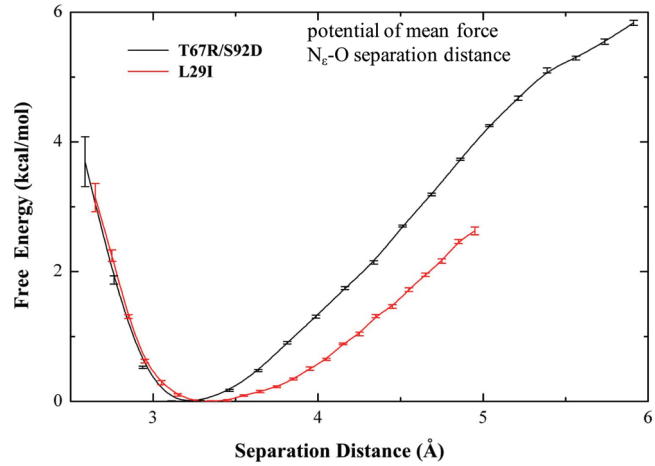

Figure 7. Potential of mean force for the N_ε-O separation distance. The black line corresponds to L29I MbCO. The red line corresponds to T67R/S92D MbCO.

ε-nitrogen maintains a constant distance from the oxygen of the CO ligand, whereas the δ-nitrogen switches between two favorable distances from the oxygen atom: approximately 3.96 and 5.39 Å (Figure 8A,B). This requires at least a local reconfiguration of the E helix, which is consistent with the suggestion made by Ishikawa et al.[4] and X-ray crystal studies.[11] The simulation results suggest a connection between the A_1−A_3 interconversion and global changes in the structure of the protein.

In addition to the fairly good numerical agreement between the predicted and observed substate interconversion time, confirmation that the structure of the protein is being modeled accurately can be found through comparison to the crystal structure. This comparison should be used cautiously because the simulations use MbCO containing the L29I mutation instead of the wild-type protein and because of the temperature difference between the simulations and the protein in the crystal structure. However, from experiment, it is believed that the effect of the L29I mutation is to push His64 farther away from the CO ligand,[38] which may leave the favorable position of the imidazole side chain's dihedral angle unchanged. Additionally, the frequencies of the IR absorption peaks for L29I are nearly identical to the wild-type absorption peak frequencies because absorption peak frequencies are highly sensitive to protein structure; this implies that the structural changes between the

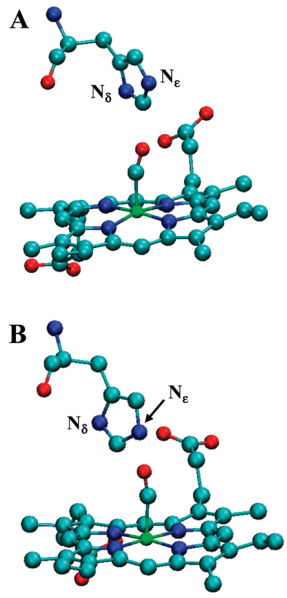

Figure 8. (A) Representative snapshot of His64 with the N_δ-O separation distance at 4.12 Å. (B) Representative snapshot of His64 with the N_δ-O separation distance at 5.06 Å. Note that the C_α-C_β-C_γ-$C_{\delta 2}$ dihedral angle in (A) is −114° and the same angle in (B) is −125°.

L29I mutant and wild type are minimal.[4] The crystal structure shows three positions for the imidazole side chain of His64, although this does not reveal how the local changes relate to larger structural changes. One of these positions has His64 swung out of the heme pocket, a configuration that corresponds to the A_0 substate.[4] The other two stable positions have dihedral angles of −121 and −122°. These angles are consistent with the −110° predicted by this study's PMF.

The PMF for the N_δ-O coordinate for the T67R/S92D mutant (Figure 5) shows only one favorable position, unlike the same coordinate for the L29I mutant, whereas the N_ε-O and C_α-C_β-C_γ-$C_{\delta 2}$ coordinates are qualitatively similar to the L29I mutant and show only one favorable position. These results predict that there would be only a single peak in the IR absorption spectrum in the frequency range that contains the A_1 and A_3 bands and no interconversion. However, as seen in Figure 1, both the A_1 and A_3 substates have significant amplitude, and fast substate interconversion is seen experimentally in the T67R/S92D mutant. (See Figures 2 and 3.)

The failure of the same three reaction coordinates used in the L29I mutant to reproduce the experimentally observed interconversion time for the T67R/S92D mutant may indicate that either the force field is in error or the true potential energy landscape for the double mutant cannot be simply described by a simple reaction coordinate (or by one of the three studied in this work). These results demonstrate that a procedure that successfully simulates dynamical behavior in one system cannot necessarily be assumed to work for other systems, even if they have minimal structural modifications. The agreement between the L29I simulations and experimental results is unlikely to be fortuitous given the wide range of time scales over which substate interconversion can occur[1,4] and the consistency between the expectation of the change in the structure of the *E*-helix[4] and the movement of the H64 backbone observed in the simulations. It should be noted that agreement between the simulations in the current study and experiments on L29I mutated MbCO as described above may provide evidence verifying a reasonable degree of accuracy of the protein force field. Additionally, comparisons between the electric field generated by the force field and partial charge parameter set used in these simulations with the electric field generated by QM/MM(MD) simulations further verify the force field. In previous studies, different reaction coordinates were used to predict an interconversion time with the same order of magnitude as that observed experimentally.[1] It was concluded that some change in the structure of the *E*-helix is likely involved in the A_1-A_3 interconversion,[4] which is consistent with the results in this study. However, the results of the present work on the T67R/S92D double mutant appear to indicate that the transition between the two substates cannot be simply described by the same structural reaction coordinate for both the L29I and T67R/S92D mutants despite the fact that the apparent structural differences are small. (It should be noted that there is no currently available crystal structure with which to compare the simulated structure of the T67R/S92D double mutant. The one available crystal structure of T67R/S92D myoglobin differs by three amino acids from the protein system studied here and has a CN ligand rather than CO.)[39]

IV. Concluding Remarks

Ultrafast 2D IR vibrational echo chemical exchange experiments have been employed to examine A_1-A_3 substate interconversion for the MbCO double mutant, T67R/S92D. The absorption spectrum shows that the CO stretching mode frequencies for the A_1 and A_3 substates are virtually identical in frequency to that of wild-type MbCO. However, the equilibrium constant is different favoring the A_3 substate over the A_1 substate (Figure 1), in contrast with wild-type MbCO in which the A_1 substate is favored. The time-dependent evolution of the 2D IR spectrum yields the $A_1 \rightarrow A_3$ substate switching time, $\tau_{13} = 1/k_{13} = 76 \pm 10$ ps (Figures 2 and 3). Previous 2D IR chemical exchange measurements for the single mutant, L29I, gave a switching time of 47 ± 8 ps.[4]

MD simulations of L29I MbCO have successfully reproduced the A_1-A_3 interconversion time within a factor of ∼2, whereas simulations of T67R/S92D have failed to reproduce the experimentally observed interconversion time (Figures 2 and 3) using the same reaction coordinates. The simulations of the double mutant indicate that there would be a single substate in the frequency range associated with the A_1 and A_3 substates in contrast with experiment. (See Figure 1.) The primary structural change seen in the L29I simulations is lateral movement of the backbone of His64 to push the δ-nitrogen of the imidazole side chain back and forth between two favorable distances from the CO ligand.

This primary structural change that produces two substates for L29I but only one for the T67R/S92D is in contrast with recent MD simulations of the double mutant[14] using the Amber 10 simulation package with the 2003 force field.[15,16] These simulations obtained the frequency-frequency correlation function (FFCF) from the fluctuating electric field along the CO bond using the Stark coupling constant as a single adjustable parameter. The FFCF is used to calculate the IR absorption spectrum and 2D IR vibrational echo data. The results yield the A_1 and A_3 bands with virtually the correct line shapes but an error of ∼33% in the separation between the two bands. The simulated FFCFs for the two bands show decay times within factors of ∼2 of the experimentally observed dynamics within each substate. However, substate interconversion is observed to be several orders of magnitude too slow. The structural change identified as being responsible for the A_1 and A_3 substates involves the orientation of the imidazole side group of H64[1,8,14] as opposed to the translation of H64 found here for L29I.

Reproducing the experimentally observed substate interconversion time of L29I represents a longstanding challenge in biophysical modeling,[40] so it is encouraging to see that the present study has made significant advances in this regard. However, the observations that (1) previous studies successfully predicted the interconversion time to the right order of magnitude using different structural coordinates[4] and (2) the same reaction coordinates that successfully showed two favorable substates for the L29I mutant in this study showed only one favorable substate in the simulations of the T67R/S92D mutant may indicate that structural transitions on the free energy landscape of the various mutants cannot be described using the same reaction coordinate, a result that points to the likely complexity of the underlying protein free energy landscape. As a result, computational analysis that may be reasonable for one mutant may not be simply transferred to another mutant without additional verification and development. Further study of this particular protein free energy landscape is, however, warranted because knowledge of the mechanism for fast substate interconversion in myoglobin may serve as a model that can be used to interpret conformational switching processes in other proteins.[4]

Acknowledgment. We thank Professor Luigi Casella, Dipartimento di Chimia Generale, University of Pavia, Italy, for providing us with the original plasmid for the Mb double mutant (T67R/S92D), which was used to obtain the plasmid employed in this work. DGT, IFT, and GAV acknowledge the National Science Foundation through grants CHE-0628257, CHE-1036464, and CHE-0649039 (REU) for support of this research. S.B. and M.D.F. acknowledge the National Institutes of Health grant 2-R01-GM061137-09 for support of this research. S.B. acknowledges partial support from the National Institutes of Health grant 5-R01-GM027738.

References and Notes

(1) Merchant, K. A.; Noid, W. G.; Akiyama, R.; Finkelstein, I. J.; Goun, A.; McClain, B. L.; Loring, R. F.; Fayer, M. D. *J. Am. Chem. Soc.* **2003**, *125*, 13804.

(2) Thorpe, I. F.; Brooks, C. L. *J. Am. Chem. Soc.* **2005**, *127*, 12997.

(3) Frauenfelder, H.; McMahon, B. H.; Austin, R. H.; Chu, K.; Groves, J. T. *Proc. Natl. Acad. Sci. U.S.A.* **2001**, *98*, 2370.

(4) Ishikawa, H.; Kwak, K.; Chung, J. K.; Kim, S.; Fayer, M. D. *Proc. Natl. Acad. Sci. U.S.A.* **2008**, *105*, 8619.

(5) Nienhaus, G. U.; Muller, J. D.; McMahon, B. H.; Frauenfelder, H. *Physica D* **1997**, *107*, 297.

(6) Hong, M. K.; Braunstein, D.; Cowen, B. R.; Frauenfelder, H.; Iben, I. E.; Mourant, J. R.; Ormos, P.; Scholl, R.; Schulte, A.; Steinbach, P. J. *Biophys. J.* **1990**, *58*, 429.

(7) Johnson, J. B.; Lamb, D. C.; Frauenfelder, H.; Müller, J. D.; McMahon, B.; Nienhaus, G. U.; Young, R. D. *Biophys. J.* **1996**, *71*, 1563.

(8) Merchant, K. A.; Thompson, D. E.; Xu, Q.-H.; Williams, R. B.; Loring, R. F.; Fayer, M. D. *Biophys. J.* **2002**, *82*, 3277.

(9) Zheng, J. R.; Kwak, K.; Asbury, J.; Chen, X.; Piletic, I. R.; Fayer, M. D. *Science* **2005**, *309*, 1338.

(10) Vojtechovsky, J.; Chu, K.; Berendzen, J.; Sweet, R. M.; Schlichting, I. *Biophys. J.* **1999**, *77*, 2153.

(11) Teeter, M. M. *Protein Sci.* **2004**, *13*, 313.

(12) Elber, R.; Karplus, M. *Science* **1987**, *235*, 318.

(13) Devereux, M.; Meuwly, M. *Biophys. J.* **2009**, *96*, 4363.

(14) Bagchi, S.; Nebgen, B. T.; Loring, R. F.; Fayer, M. D. *J. Am. Chem. Soc.*, accepted.

(15) Case, D. A. *Amber 10*; University of California: San Francisco, 2008.

(16) Giammona, D. A. *Heme Parameters*; University of California, Davis: Davis, CA, 1984.

(17) Souaille, M.; Roux, B. *Comput. Phys. Commun.* **2001**, *135*, 40.

(18) Brooks, B. R.; Brooks, C. L.; Mackerell, A. D.; Nilsson, L.; Petrella, R. J.; Roux, B.; Won, Y.; Archontis, G.; Bartels, C.; Boresch, S.; Caflisch, A.; Caves, L.; Cui, Q.; Dinner, A. R.; Feig, M.; Fischer, S.; Gao, J.; Hodoscek, M.; Im, W.; Kuczera, K.; Lazaridis, T.; Ma, J.; Ovchinnikov, V.; Paci, E.; Pastor, R. W.; Post, C. B.; Pu, J. Z.; Schaefer, M.; Tidor, B.; Venable, R. M.; Woodcock, H. L.; Wu, X.; Yang, W.; York, D. M.; Karplus, M. *J. Comput. Chem.* **2009**, *30*, 1545.

(19) MacKerell, A. D.; Bashford, D.; Bellott, M.; Dunbrack, R. L.; Evanseck, J. D.; Field, M. J.; Fischer, S.; Gao, J.; Guo, H.; Ha, S.; Joseph-McCarthy, D.; Kuchnir, L.; Kuczera, K.; Lau, F. T. K.; Mattos, C.; Michnick, S.; Ngo, T.; Nguyen, D. T.; Prodhom, B.; Reiher, W. E.; Roux, B.; Schlenkrich, M.; Smith, J. C.; Stote, R.; Straub, J.; Watanabe, M.; Wiorkiewicz-Kuczera, J.; Yin, D.; Karplus, M. *J. Phys. Chem. B* **1998**, *102*, 3586.

(20) Grossfield, A.

(21) Ryckaert, J. P.; Ciccotti, G.; Berendsen, H. J. C. *J. Comput. Phys.* **1977**, *23*, 327.

(22) Darden, T.; York, D.; Pedersen, L. *J. Chem. Phys.* **1993**, *98*, 10089.

(23) Kwak, K.; Zheng, J. R.; Cang, H.; Fayer, M. D. *J. Phys. Chem. B* **2006**, *110*, 19998.

(24) Park, S.; Kwak, K.; Fayer, M. *Laser Phys. Lett.* **2007**, *4*, 704.

(25) Zheng, J. R.; Kwak, K. W.; Xie, J.; Fayer, M. D. *Science* **2006**, *313*, 1951.

(26) Asbury, J. B.; Steinel, T.; Fayer, M. D. *J. Lumin.* **2004**, *107*, 271.

(27) Rector, K. D.; Kwok, A. S.; Ferrante, C.; Tokmakoff, A.; Rella, C. W.; Fayer, M. D. *J. Chem. Phys.* **1997**, *106*, 10027.

(28) Golonzka, O.; Khalil, M.; Demirdöven, N.; Tokmakoff, A. *Phys. Rev. Lett.* **2001**, *86*, 2154.

(29) Ishikawa, H.; Finkelstein, J.; Kim, S.; Kwak, K.; Chung, J. K.; Wakasugi, K.; Massari, A. M.; Fayer, M. D. *Proc. Natl. Acad. Sci. U.S.A.* **2007**, *104*, 16116.

(30) Ishikawa, H.; Kim, S.; Kwak, K.; Wakasugi, K.; Fayer, M. D. *Proc. Natl. Acad. Sci. U.S.A.* **2007**, *104*, 19309.

(31) Zheng, J.; Kwak, K.; Chen, X.; Fayer, M. D. *J. Am. Chem. Soc.* **2006**, *128*, 2977.

(32) Kwak, K.; Zheng, J.; Cang, H.; Fayer, M. D. *J. Phys. Chem. B* **2006**, *110*, 19998.

(33) Zheng, J.; Fayer, M. D. *J. Am. Chem. Soc.* **2007**, *129*, 4328.

(34) Zheng, J.; Fayer, M. D. *J. Phys. Chem. B* **2008**, *112*, 10221.

(35) Kwak, K.; Rosenfeld, D. E.; Chung, J. K.; Fayer, M. D. *J. Phys. Chem. B* **2008**, *112*, 13906.

(36) Moilanen, D. E.; Wong, D.; Rosenfeld, D. E.; Fenn, E. E.; Fayer, M. D. *Proc. Natl. Acad. Sci. U.S.A.* **2009**, *106*, 375.

(37) Maupin, C. M.; McKenna, R.; Silverman, D. N.; Voth, G. A. *J. Am. Chem. Soc.* **2009**, *131*, 7598.

(38) Li, T.; Quillin, M. L.; Phillips, G. N.; Olson, J. S. *Biochemistry* **1994**, *33*, 1433.

(39) Roncone, R.; Monzani, E.; Murtas, M.; Battaini, G.; Pennati, A.; Sanangelanton, A. M.; Zuccotti, S.; Bolognesi, M.; Casella, L. *Biochem. J.* **2004**, *717−724*, 717.

(40) Merchant, K. A.; Noid, W. G.; Thompson, D. E.; Akiyama, R.; Loring, R. F.; Fayer, M. D. *J. Phys. Chem. B* **2002**, *107*, 4.

JP109203B